Hindawi
Shock and Vibration
Volume 2020, Article ID 8342041, 15 pages
https://doi.org/10.1155/2020/8342041

Research Article

A Novel Method to Reduce the Laser Drilling Time for Hole Cluster considering the Influence of Residual Vibration of the Sample Stage

Xiaodong Wang,[1,2] Bin Liu,[1,2] Xuesong Mei,[1,2] Jun Yang,[1,2] Xialun Yun,[1,2] Xiao Li,[1,2] and Jian Li[3]

[1]*State Key Laboratory for Manufacturing Systems Engineering, Xi'an 710049, China*
[2]*Shaanxi Key Laboratory of Intelligent Robots, Xi'an 710049, China*
[3]*School of Mechatronics Engineering, Henan University of Science and Technology, Luoyang 471003, China*

Correspondence should be addressed to Bin Liu; liubin1110@xjtu.edu.cn

Received 16 January 2020; Revised 9 May 2020; Accepted 6 June 2020; Published 29 June 2020

Academic Editor: Dario Di Maio

Copyright © 2020 Xiaodong Wang et al. This is an open access article distributed under the Creative Commons Attribution License, which permits unrestricted use, distribution, and reproduction in any medium, provided the original work is properly cited.

In large areas of laser drilling, the residual vibration occurs when the sample stage moves in PTP (Point to Point) movement. It affects the surface quality and processing efficiency of the holes. The common solution for this problem is to set the laser irradiation delay time by the controller to wait for the residual vibration attenuation, but the whole drilling circle will increase. In this paper, a new method is introduced to reduce the laser drilling circle. By setting the allowable threshold of the residual vibration for the subsequent process, the sum of the time in deceleration segment of the trapezoidal moving profile, and the time when the residual vibration attenuates below the amplitude threshold (ST) can be minimized as the optimization goal. The results show that for a given operating speed, there is always an optimum acceleration value for the deceleration segment of the trapezoidal moving profile, which minimizes the ST value. Further, the delay time for laser irradiation can also be estimated according to the optimal acceleration during laser drilling.

1. Introduction

Laser processing holds the characteristics of noncontact, low pollution, and high efficiency. In recent years, with the development of laser technology, laser processing has become ever more in-depth in the fields of welding [1–3], hard or brittle material cutting [4–7], drilling [8–12], and surface structure texturing [13–15]. The performance requirements of laser processing products are higher and higher, such as ultracomplex structure, super surface of hydrophobic and oleophobic and high aspect ratio microholes, etc., which induces higher performance requirements for laser processing equipment. Laser processing equipment is usually integrated by laser systems, motion control systems, optical path systems, and galvanometer systems. These subsystems are usually produced by different manufacturers and are relatively independent, which is necessary to be effectively integrated. Laser processing is achieved through cooperative control between these subsystems. The delay problem in the cooperative control process determines the performance of the equipment and affects the processing efficiency. It is of profound significance to reduce the delay problem in the cooperative control process. For a better understanding, Table 1 provides an explanation of the abbreviations in this paper.

Figure 1(a) shows a common laser processing equipment that is equipped with a laser source, a galvanometer, and a motion control system. Figure 1(b) shows the common PTP path for laser drilling. Figure 1(c) is the schematic diagram of the vibration of the laser beam relative to the workpiece caused by residual vibration. Usually, the sample stage achieves motion positioning and then the galvanometer

Table 1: Abbreviation description.

Abbreviation	Abbreviation meaning
ST	The sum of the time in the deceleration segment of the trapezoidal moving profile and the time when residual vibration decays below the amplitude threshold
ARMA	Autoregressive moving average
STD	Sparse time domain
AS	Acceleration signal
FVS	Free vibration signal/residual vibration signal
FVSF	Free vibration signal filtering
PSD	Self-power spectrum
AFS	Signal after low-pass filtering
RVT	Residual vibration threshold
Acc	Acceleration
EC	Envelope curve

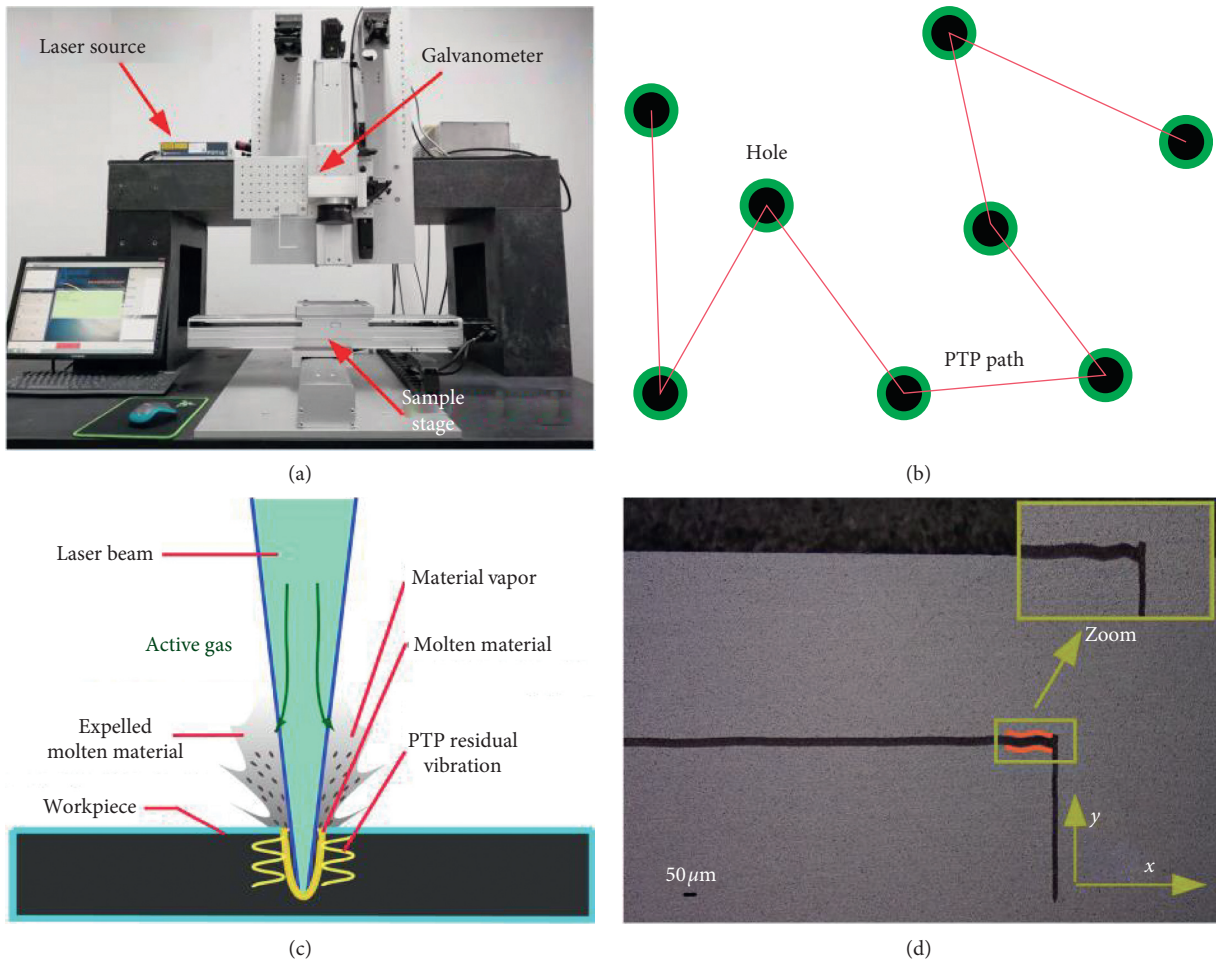

Figure 1: Schematic diagram of laser drilling. (a) Laser processing equipment; (b) PTP motion; (c) PTP residual vibration in laser drilling; (d) Residual vibration at the corner of the machining path.

controls the laser drilling. When the galvanometer is positioned, the controller triggers the laser shutter to emit several laser pulses for drilling. However, the completion of positioning action is always accompanied by the generation of residual vibration, as shown in Figure 1(d). The effect of vibration on holes' quality is not negligible if the laser is turned on immediately, especially when the design size of the hole is small. The common solution to this problem is to set the laser irradiation delay so that the laser pulses are irradiated after the attenuation of the residual vibration [16]. When the motion actuator is a robot arm, the residual vibration tends to be larger and the decay time is longer, which seriously affects the entire drilling efficiency [17, 18].

Nowadays, in the field of laser drilling, many motion controllers still use the simple trapezoidal moving profile to control the motion of the sample stage due to the complexity

of motion control algorithms and product cost. Although this type of move profile is simple and easy to be operated, residual vibration will inevitably occur when the sample stage stops, which affects the processing quality and processing efficiency [19–21]. The residual vibration is related to the deceleration section of the trapezoidal moving profile. So how to effectively control the acceleration value of the deceleration section to make the motion positioning time and the delay time for laser irradiation shortest is of great significance for shortening the whole drilling cycle. At present, most scholars' researches focus on how to eliminate the residual vibration and they have done a lot of meaningful researches. Some scholars studied the high-order trajectory smoothing algorithm, such as the fifth-order polynomial trajectory to make the acceleration and jerk (the derivative of acceleration with time) continuous, so as to reduce the acceleration fluctuation during the motion [22]. Some scholars study the optimization algorithm to minimize the energy of the jerk for the whole running trajectory under certain speed and acceleration constraints. Then the obtained jerk trajectory is used to generate smooth acceleration and velocity trajectory, which make the sample stage run smoother [23–25]. Some scholars use filtering methods such as low-pass filtering, band-pass filtering, input shaping, etc. to make the spectrum of the acceleration trajectory have lower energy near the natural frequency of the sample stage, thereby reducing the vibration during the motion of the table [26–29]. There are also some scholars using feedforward plus feedback control to improve servo performance. The residual vibration is regarded as the disturbing term to the command position. The filter model needed to eliminate the residual vibration is obtained by solving the inverse model of the system dynamics model [30–32].

All of the above researches are considered to reduce residual vibration completely by modulating the acceleration during motion. There is no guarantee that these methods will make the whole processing time smaller, but it may make the time larger. Moreover, the methods above researches need to be written to the motion controller before used, which is time-consuming and laborious and very difficult for the laser application. Most motion controllers in the laser drilling field are closed to the user at the control algorithm level and do not support user-defined motion control algorithms. Otherwise, it may cause security risks [33].

In actual laser drilling, the trapezoidal moving profile is the most common velocity profile and almost all controllers support this velocity profile. In fact, when the residual vibration is attenuated to a certain amplitude which does not affect the quality of the sample, the laser can be irradiated. The decay time of the residual vibration is related to the magnitude of the excitation force when the motion stage is stopped, that is to say, it is related to the magnitude of the acceleration value of the deceleration section. Therefore, there may be an acceleration value to let the ST get the minimum, so as to shorten the whole drilling circle. In this paper, the problem is deeply studied from the perspective of shortening the whole drilling cycle rather than from the perspective of eliminating the residual vibration. The ST value is minimized as the optimization goal, and the optimal acceleration is obtained. The results demonstrate that the optimum acceleration of the deceleration section is only related to the dynamic parameters of the sample stage at a given operating speed. When the dynamic parameters are obtained, the optimal acceleration of the deceleration section is just set according to the speed. The optimal delay time before laser irradiation can also be estimated according to the optimal acceleration.

The content of this paper is organized as follows. The second part gives the model of the impulse response for the second-order underdamped system and the system parameters identification method based on the ARMA (autoregressive moving average) method. The third part gives the method for reducing the ST value proposed in this paper. The fourth part introduces the experimental design and experimental equipment of this paper and explains the system parameters identification results based on ARMA. Then the experimental results of the method for reducing the whole laser drilling circle in this paper are given. The last part gives the conclusions of this paper.

2. Residual Vibration Description and Identification of System Dynamics Parameters

2.1. Second-Order Underdamped System Dynamics Model. Figure 2 is a schematic diagram of the mechanical dynamics such as the sample stage, which can be described by a typical second-order system.

The transfer function of a typical second-order system can be described as follows:

$$G(s) = \frac{w_n^2}{s^2 + 2\xi w_n s + w_n^2}, \tag{1}$$

where ω_n is the undamped natural frequency and ξ is the damping ratio. For a second-order underdamped system, $0 < \xi < 1$, and ξ determines the degree of vibration attenuation of the system, and ω_n determines the period of vibration attenuation [33].

When the sample stage moves in a trapezoidal moving profile, the residual vibration occurs at the moment the sample stage stops. The form of the residual vibration usually appears as the attenuation vibration of a second-order underdamped system for the impulse input. By identifying the parameters of the system model, the residual vibration can be mathematically described, which provide conditions for the planning algorithms of optimal move profile in further time.

The response of the second-order system to the input can be expressed as follows:

$$Y(s) = G(s)U(s). \tag{2}$$

When $U(s) = K$, that is, the input is a pulse signal, the output $Y(s) = KG(s)$, then the time response signal of the second-order system for the pulse input is obtained by inverse Laplace transform:

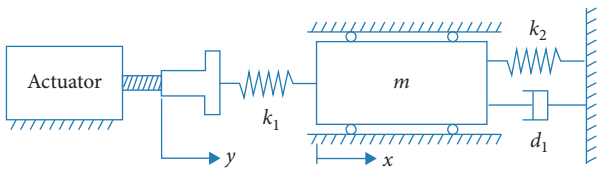

Figure 2: Schematic diagram of the mechanical system dynamics analysis.

$$\begin{aligned} y(t) &= L^{-1}(Y(s)) \\ &= L^{-1}\left(K\frac{w_n^2}{s^2+2\xi w_n s+w_n^2}\right) \\ &= K\frac{w_n^2}{\sqrt{w_n^2-(\xi w_n)^2}}e^{-\xi w_n t}\sin\left(\sqrt{w_n^2-(\xi w_n)^2}\times t\right). \end{aligned} \tag{3}$$

Let

$$x = [x(1)\,x(2)\,x(3)]^T = \left[w_n^2\;\xi w_n\;K\right]^T. \tag{4}$$

Then

$$y(t) = x(3)\frac{x(1)}{\sqrt{x(1)-x(2)^2}}e^{-x(2)\times t}\sin\left(\sqrt{x(1)-x(2)^2}\times t\right). \tag{5}$$

Using system identification algorithms such as ARMA, STD (sparse time domain), etc., the model parameters can be obtained through the measurement and analysis of the residual vibration signal.

2.2. ARMA Time Series Analysis Method for Solving System Parameters. In the process of obtaining the dynamic parameters of the sample stage, the self-excited force generated by the high-speed impact of the sample stage is used to generate the residual vibration, and the residual vibration signal is collected. The ARMA time series analysis method is used to obtain the inherent spectrum and damping coefficient of the sample stage. Compared with the traditional hammer method, the parameter identification method based on residual vibration signal analysis can better describe the system state in the actual working environment [34, 35].

The ARMA time series analysis method is a method for describing the ordered random vibration data by using model parameters, thereby obtaining system parameters; the details of this method being available in the literature [36, 37]. The parametric model includes an autoregressive (AR) model and a moving average (MA) model. The AR model describes the dynamic characteristics of the system and the MA moving is related to external disturbances and inputs. Usually, a system model composed by a p-order AR model and a q-order MA model can be expressed as ARMA(p, q), and its expression is as follows:

$$x_t - \sum_{i=1}^{p}\phi_i x_{t-i} = \sum_{l=0}^{q}\theta_l\varepsilon_{t-l}. \tag{6}$$

In the above expression, x_t is the time domain signal, ϕ_i is the autoregressive coefficient, θ_l is the moving average coefficient, and ε_t is the white noise.

Since the ARMA process $\{x_t\}$ has a unique stationary solution expressed by the following:

$$x_t = \sum_{j=0}^{\infty}G_j\varepsilon_{t-j}. \tag{7}$$

Then

$$x_{t-k} = \sum_{j=0}^{\infty}G_j\varepsilon_{t-j-k}. \tag{8}$$

In equation (7), G_j is an impulse response function.

From equations (6) and (8), the following expressions can be derived:

$$x_t x_{t-k} - \sum_{i=1}^{p}\phi_i x_{t-i}x_{t-k} = \sum_{l=0}^{q}\theta_l\varepsilon_{t-l}\sum_{j=0}^{\infty}G_j\varepsilon_{t-j-k}, \tag{9}$$

$$\begin{aligned} E(x_t x_{t-k}) - E\left(\sum_{i=1}^{p}\phi_i x_{t-i}x_{t-k}\right) &= E\left(\sum_{l=0}^{q}\theta_l\varepsilon_{t-l}\sum_{j=0}^{\infty}G_j\varepsilon_{t-j-k}\right) \\ &= \sum_{l=0}^{q}\sum_{j=0}^{\infty}\theta_l G_j E\left(\varepsilon_{t-l}\varepsilon_{t-j-k}\right). \end{aligned} \tag{10}$$

In the above expression, the item $E(x_t\,x_{t-k})$ is the k-order autocorrelation function of the time domain signal x_t and can be expressed by r_k. The item $E(\varepsilon_{t-l}\,\varepsilon_{t-j-k})$ is the k-order autocorrelation function of the white noise and can be expressed by the following:

$$E\left(\varepsilon_{t-l}\varepsilon_{t-j-k}\right) = \begin{cases} \sigma^2, & (l = j+k), \\ 0, & (\text{others}). \end{cases} \tag{11}$$

The σ^2 is the variance of the white noise.

It can be further derived from equations (10) and (11)

$$r_k - \sum_{i=1}^{p}\phi_i r_{k-i} = \sigma^2\sum_{j=0}^{\infty}\theta_{k+j}G_j. \tag{12}$$

In the above expression, when $j<0$, $G_j=0$. When $l=k+j\notin\{1, 2, \ldots, q\}$, $\theta_l=0$. The r_k is the k-order autocorrelation function of the time domain signal. Usually, the difference order k of the ARMA model satisfies $k\gg\max(p, q+1)$, which means $k+j\gg q$, then the right term in equation (12) is equal to 0, which gives the following:

$$r_k - \sum_{i=1}^{p}\phi_i r_{k-i} = 0, \quad k\geq M = \max(p, q+1). \tag{13}$$

Let the length of the autocorrelation function be L. Usually, L is much larger than M. Then, the following expressions can be derived:

$$\begin{cases} r_M = \phi_1 r_{M-1} + \phi_2 r_{M-2} + \cdots + \phi_p r_{M-p}, \\ r_{M+1} = \phi_1 r_M + \phi_2 r_{M-1} + \cdots + \phi_p r_{M-p+1}, \\ \vdots \\ r_L = \phi_1 r_{L-1} + \phi_2 r_{L-2} + \cdots + \phi_p r_{L-p}, \end{cases} \tag{14}$$

which is as follows:

$$\underbrace{\begin{bmatrix} r_M \\ r_{M+1} \\ \vdots \\ r_L \end{bmatrix}}_{R'_{(L-M)\times 1}} = \underbrace{\begin{bmatrix} r_{M-1} & r_{M-2} & \cdots & r_{M-p} \\ r_M & r_{M-1} & \cdots & r_{M-p+1} \\ \vdots & \vdots & \vdots & \vdots \\ r_{L-1} & r_{L-2} & \cdots & r_{L-p} \end{bmatrix}}_{R_{(L-M)\times p}} \underbrace{\begin{bmatrix} \phi_1 \\ \phi_2 \\ \vdots \\ \phi_p \end{bmatrix}}_{\phi_{(L-M)\times 1}}. \tag{15}$$

Let $R = R_{(L-M)\times P}$, $R' = R'_{(L-M)\times 1}$, $\phi = \phi_{(L-M)\times 1}$. So the autoregressive coefficient ϕ can be expressed as follows:

$$\phi = \left(R^T R\right)^{-1}\left(R^T R'\right). \tag{16}$$

When the autoregressive coefficient ϕ_k is obtained, the dynamic parameters of the system can be calculated by the transfer function expression of the ARMA model. The transfer function form of the ARMA model is expressed as follows:

$$H(z) = \frac{\sum_{l=0}^{q} \theta_l z^{-l}}{\sum_{i=1}^{p} \phi_i z^{-i}}. \tag{17}$$

The characteristic equation of the above formula can be expressed as follows:

$$z^p + \phi_1 z^{p-1} + \cdots + \phi_p = 0. \tag{18}$$

The relationship between the transfer function poles and the system dynamics parameters can be expressed as in the following equation, in which z_k is the conjugate of z_k^*:

$$\begin{cases} z_k = e^{s_k \Delta t} = e^{\left(-w_k \xi_k + j w_k \sqrt{1-\xi_k^2}\right)\Delta t}, \\ z_k^* = e^{s_k^* \Delta t} = e^{\left(-w_k \xi_k - j w_k \sqrt{1-\xi_k^2}\right)\Delta t}. \end{cases} \tag{19}$$

The expression of the modal frequency w_k and damping ratio ξ_k can be obtained from equation (19), as shown in the following equation, where s_k is the k-order modal frequency and Δt is the sampling interval:

$$\begin{cases} w_k = \dfrac{|R_k|}{\Delta t}, \\ \xi_k = \sqrt{\dfrac{1}{1 + \left(\mathrm{Im}(R_k)/\mathrm{Re}(R_k)\right)^2}}, \\ R_k = \ln z_k = s_k \Delta t. \end{cases} \tag{20}$$

3. Time Optimal Trapezoidal Moving Profile under Residual Vibration Threshold

For the PTP motion using the trapezoidal moving profile, it is not true that the larger the acceleration value of the deceleration section is, the shorter the time for the PTP motion is, if the attenuation time of the residual vibration should be considered. For example, in the field of precision laser drilling, the residual vibration often has an influence on the shape of the hole [38]. Therefore, it is necessary to set a settling time to reduce the influence of residual vibration. Generally, the greater the acceleration of the deceleration section is, the shorter the time taken by the deceleration section will be, but the larger the amplitude of the residual vibration will be and the longer the settling time is required. It is of great significance to set the optimal acceleration value of the deceleration section to obtain the minimum ST value.

Figure 3 is a schematic diagram of the residual vibration of the trapezoidal move profile. The motion profile indicated by the red and blue curves is different only in the acceleration value of the deceleration section. The distance S_{des} of the PTP motion and the maximum speed $V_{\max}$ remain constant. Assuming that the positioning time ST is $T_{\_}$, the following expression can be achieved when there is a constant velocity segment:

$$T_{a\_} = \frac{V_{\max}}{a_{\_}}, \tag{21}$$

$$T_{\_} = T_{a\_} + T_v = \frac{V_{\max}}{a_{\_}} + T_v(a_{\_}). \tag{22}$$

In equation (22), $T_{a\_}$ represents the deceleration period time, and T_v represents the time required for the residual vibration to decay below the set threshold. Obviously, when the acceleration section adopts the same acceleration and the set operation speed is constant, the positioning cycle T takes the minimum value $T_{\min}$ when the $T_{\_}$ takes its minimum value. Thereby, for a complete trapezoidal move profile, it is only to require the minimum value $T_{\_}$ to minimize the total positioning cycle T.

As can be seen from Figure 3, at the moment of the sample stage stops, the acceleration will be abrupt, resulting in an instantaneous inertial force that acts on the sample stage and causing the residual vibration of the table.

The following expression can be obtained by Newton's second law:

$$F = ma_{\_} = \frac{mV_{\max}}{T_{a\_}}. \tag{23}$$

In the case of a certain $V_{\max}$, the larger the $a_{\_}$ is, the smaller the $T_{a\_}$ will be. As can be seen from equation (23), the larger the F will be, which will cause the larger impact, then the longer the time T_v when the residual vibration reaches the set amplitude threshold will be. Therefore, there should be an optimal acceleration $a_{\_}^*$ to make $T_{\_}$ get the minimum value $T_{\_\min}$:

$$T_{\_\min} = T_{a\_} + T_v = \frac{V_{\max}}{a_{\_}^*} + T_v(a_{\_}^*). \tag{24}$$

For the impulse response of the second-order underdamped system, the envelope exhibits the characteristic of the exponential decay curve, as shown in Figure 4. The

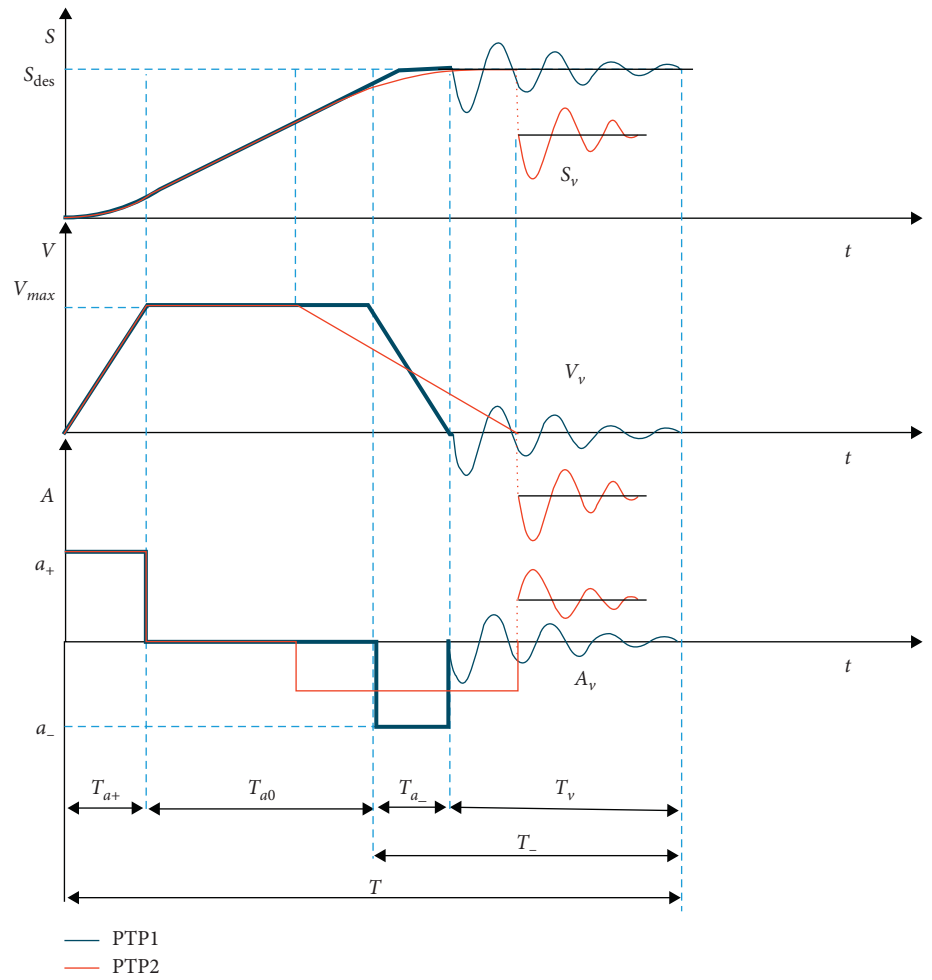

Figure 3: Schematic diagram of the residual vibration of the trapezoidal moving profile.

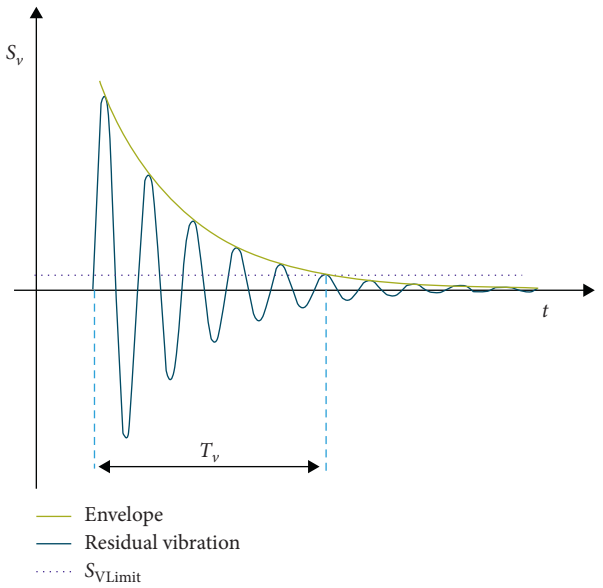

Figure 4: Residual vibration envelope.

envelope of the oscillation can be expressed by the following equation:

$$y^e(t) = K\frac{w_n^2}{\sqrt{w_n^2 - (\xi w_n)^2}}e^{-\xi w_n t}, \\ = x(3)\frac{x(1)}{\sqrt{x(1) - x(2)^2}}e^{-x(2)t}, \tag{25}$$

with $x = [x(1)x(2)x(3)] = [w^2\xi w_n K]$.

Assuming that the amplitude threshold allowed by the process is S_{Vlimit} and the relationship between the proportional coefficient K for the impulse response and the acceleration value a_- of the deceleration section is as the following equation, λ is the proportional coefficient between K and acceleration a_-:

$$x(3) = K = \lambda a_- = \lambda\frac{V_{\max}}{T_{a-}} \tag{26}$$

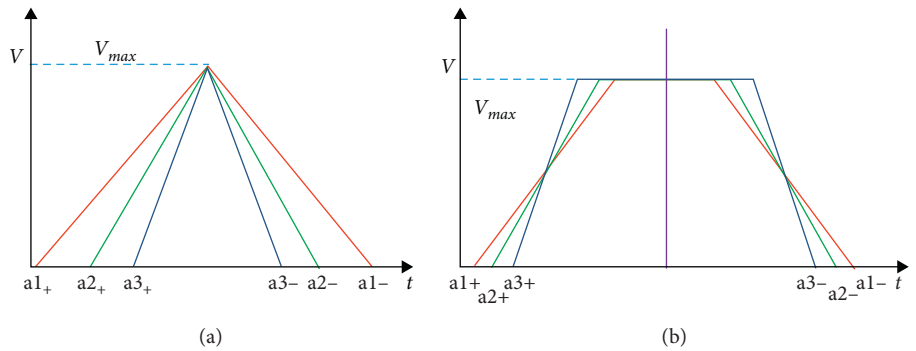

Figure 5: Two different impact forms. (a) Triangular move profile; (b) trapezoidal move profile.

If

$$y^e(T_v) = x(3)\frac{x(1)}{\sqrt{x(1)-x(2)^2}}e^{-x(2)T_v} = S_{\text{Vlimit}}. \tag{27}$$

Then, the following expression can be obtained from equations (26) and (27):

$$\begin{aligned} T_- &= T_{a_-} + T_v \\ &= T_{a_-} - \frac{1}{x(2)}\ln\left(\frac{\sqrt{x(1)-x(2)^2}\,S_{\text{Vlimit}}}{x(1)x(3)}\right) \\ &= T_{a_-} - \frac{1}{x(2)}\ln\left(\frac{T_{a_-}\sqrt{x(1)-x(2)^2}\,S_{\text{Vlimit}}}{\lambda x(1)V_{\max}}\right). \end{aligned} \tag{28}$$

Let $\partial T_-/\partial T_{a_-} = 0$, the following equations can be obtained:

$$\begin{aligned} \partial T_-/\partial T_{a_-} &= 1 - \partial\left(\frac{1}{x(2)}\ln\left(\frac{T_{a_-}\sqrt{x(1)-x(2)^2}\,S_{Vlimit}}{\lambda x(1)V_{\max}}\right)\right)/\partial T_{a_-} \\ &= 1 - \frac{1}{x(2)T_{a_-}} = 0, \end{aligned} \tag{29}$$

$$T_{a_-} = \frac{1}{x(2)} = \frac{1}{\xi w_n}. \tag{30}$$

It can be seen from equation (30) that when $T_{a_-} = 1\backslash\xi w_n, T_-$ takes the minimum value. The required acceleration a_- is represented by the following equation:

$$a_- = \frac{V_{\max}}{T_{a_-}} = V_{\max}\xi w_n. \tag{31}$$

It can be seen that for the different speeds $V_{\max}$, there is always an optimal acceleration a_- to guarantee the shortest execution time of PTP movement in the case of meeting the residual vibration threshold requirement. It also shows that the optimal value is dependent on the system dynamics parameters ω_n and ξ.

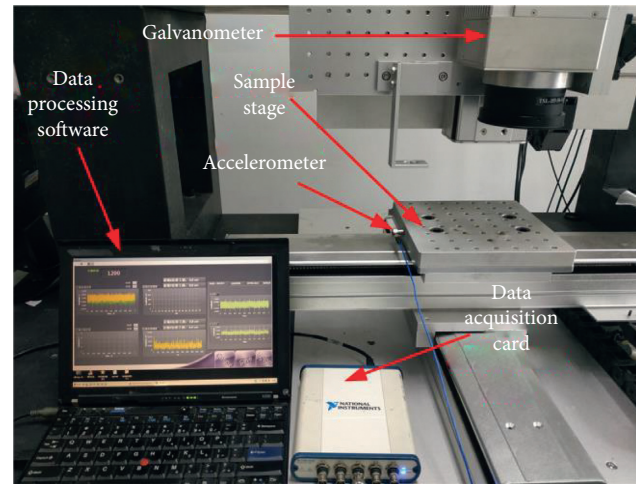

Figure 6: Experimental measurement.

4. Experiment

In order to obtain the dynamic parameters of the sample stage, two different move profiles are used to excite the sample stage, and the residual vibration signal after the sample stage stops is obtained by the signal acquisition device. The designed moving profiles are shown in Figure 5, which adopts a triangular motion profile and trapezoidal motion profile, respectively. The experimental setup is illustrated in Figure 6. The data acquisition equipment belongs to the NI company, and the data acquisition software is developed based on the LabVIEW environment. During the experiment, the sampling frequency is set as 1000 Hz. The acceleration sensor is ICP acceleration sensor. The measurement frequency range is 0.5–10000 Hz. The acceleration range is ±50 g. The machine tool is a three-axis ultraviolet nanosecond laser processing equipment, including a sample stage, a galvanometer, and so on.

Figure 7 shows the results of the residual vibration in the triangular moving profile, and Figure 8 shows the results in the trapezoidal move profile. It can be seen that the sample stage stops accompanied by the residual vibration, which is as shown by the curve FVSF. The larger the acceleration of the deceleration section is, the larger the amplitude of the residual vibration will be.

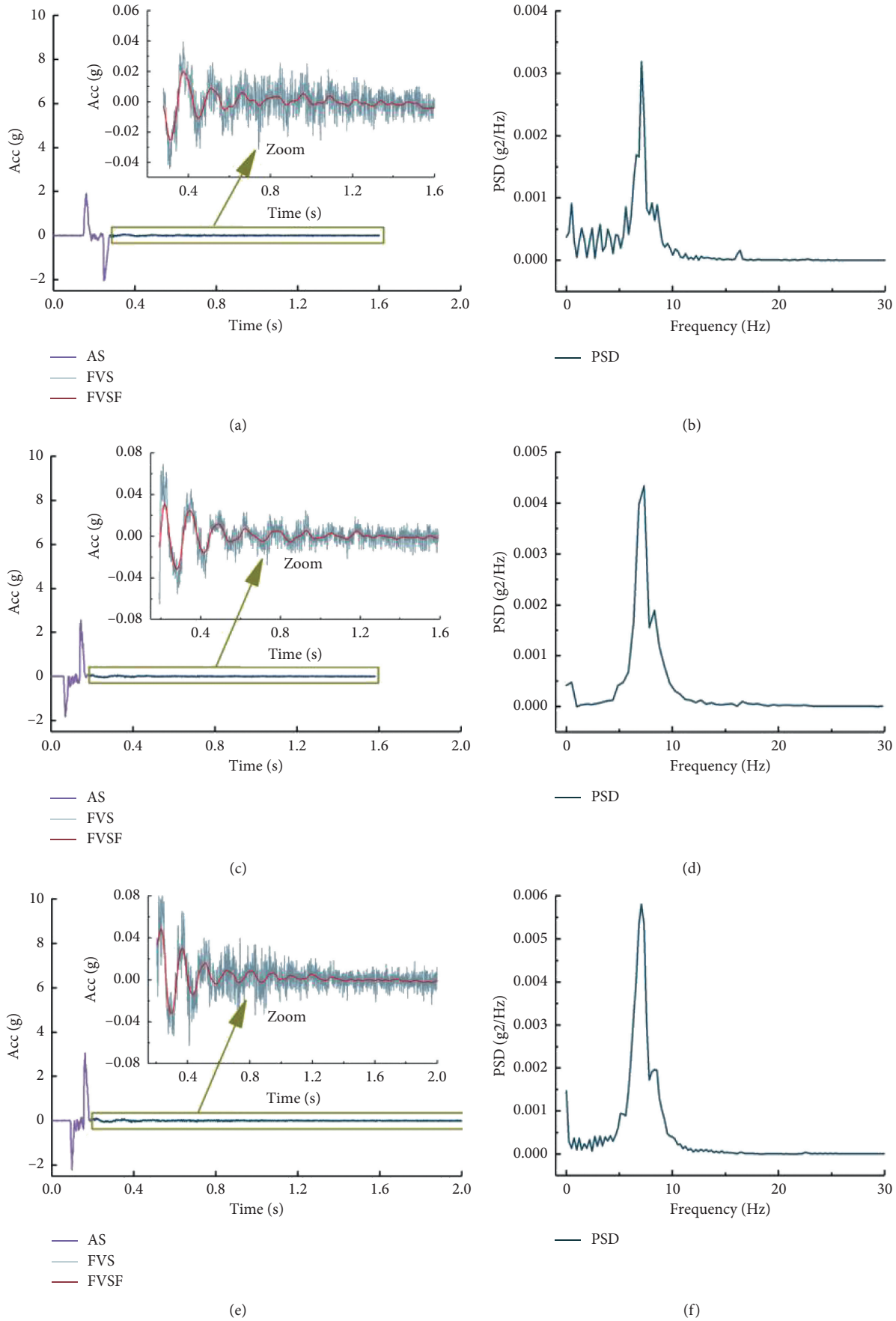

Figure 7: Residual vibration signal and PSD of FVSF for triangular move profile impact with $V_{max} = 0.8\ m\ s^{-1}$ and different $a\_$. (a) and (b) $a\_ = 2\ g$; (c) and (d) $a\_ = 2.5\ g$; (e) and (f) $a\_ = 3\ g$.

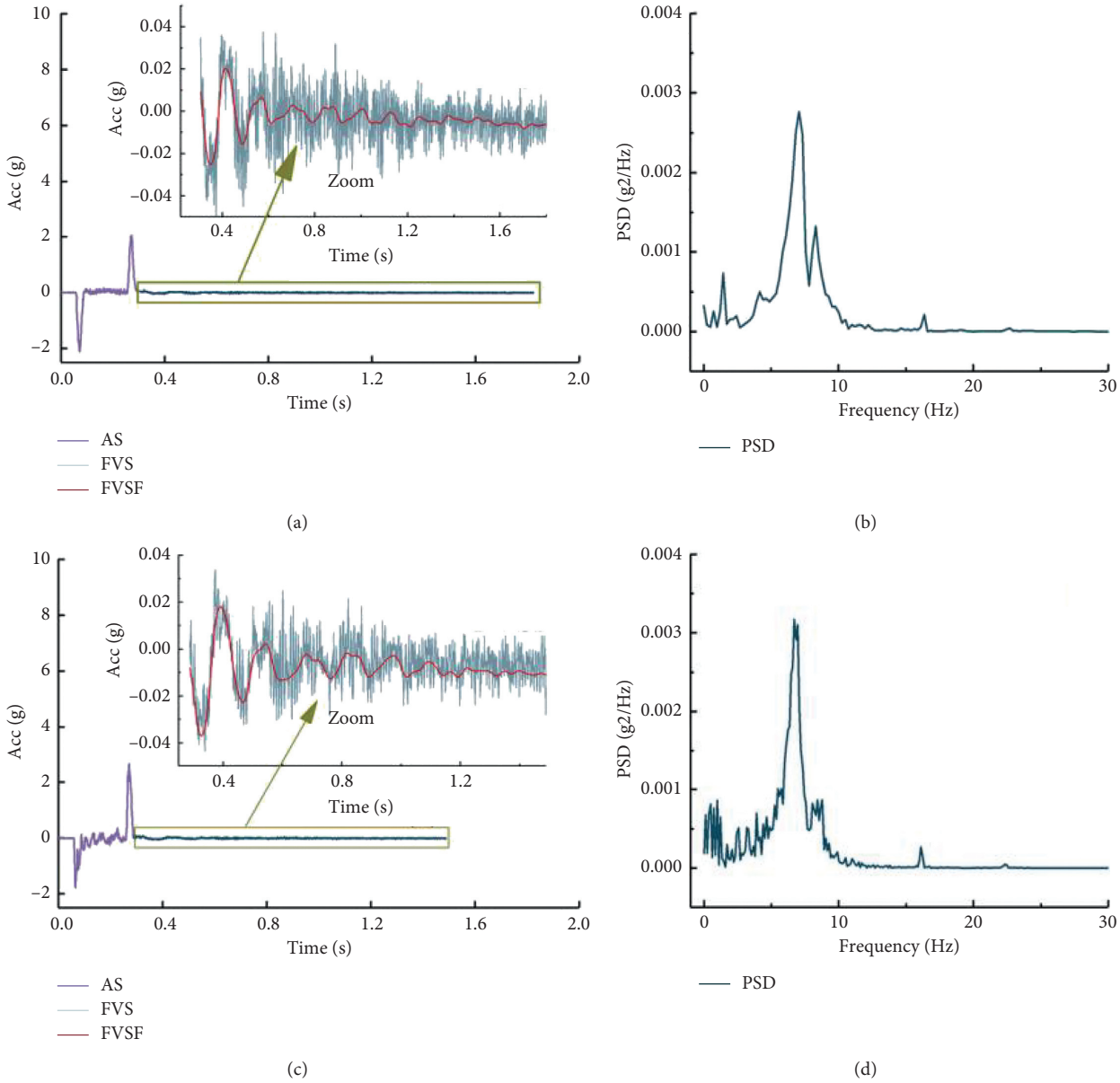

Figure 8: Continued.

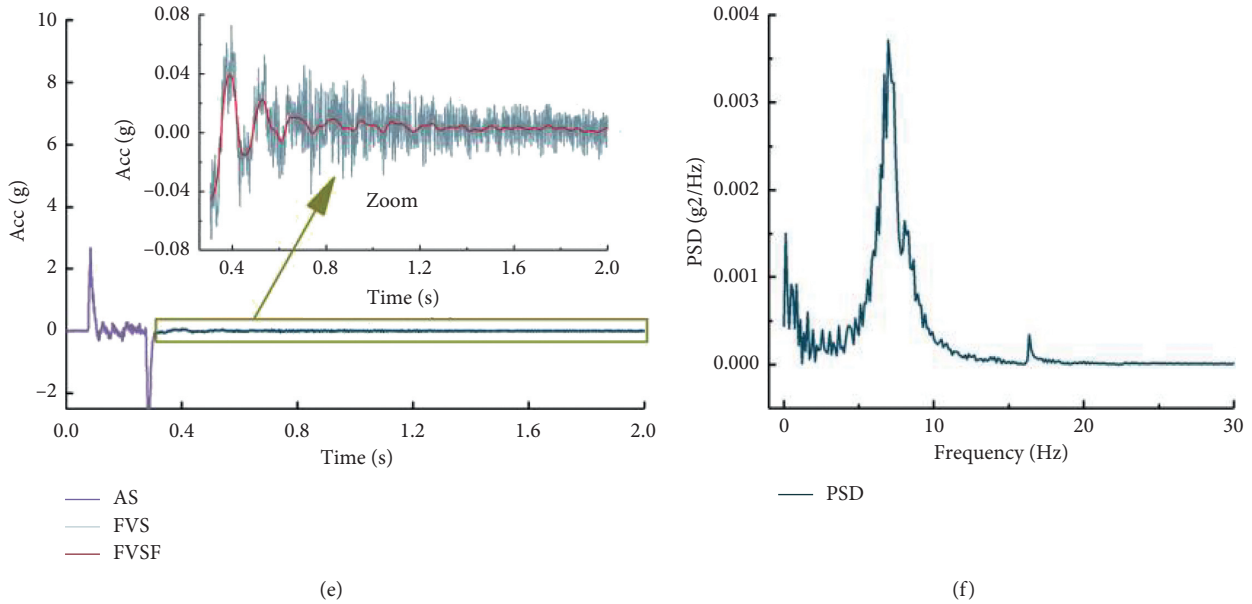

FIGURE 8: Residual vibration signal and PSD of FVSF for trapezoidal move profile impact with $V_{max} = 0.3\ m\ s^{-1}$ and different $a_{\_}$. (a) and (b) $a_{\_} = 2\ g$; (c) and (d) $a_{\_} = 2.5\ g$; (e) and (f) $a_{\_} = 3\ g$.

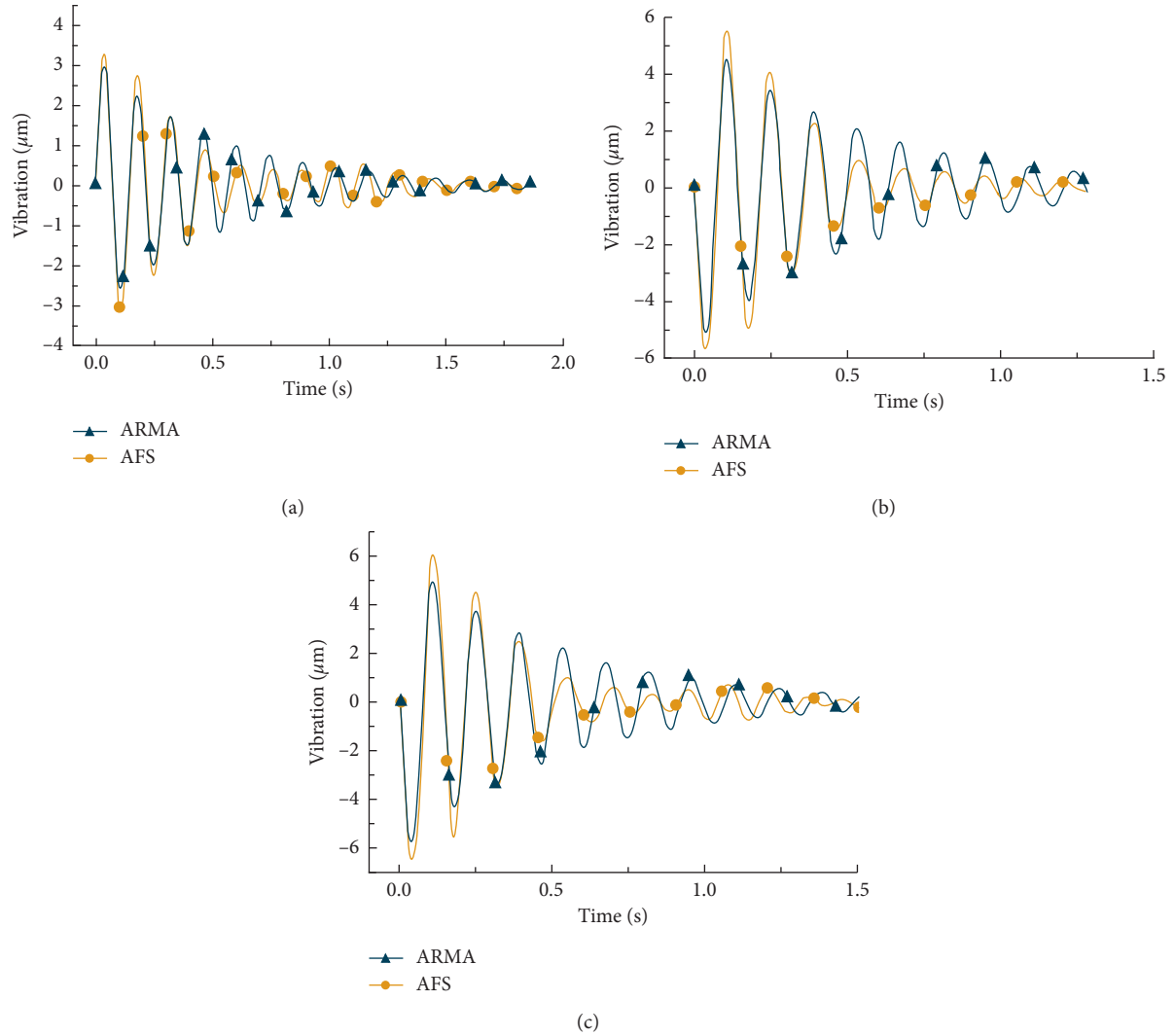

FIGURE 9: ARMA recognition results of triangle move profile impact with $V_{max} = 0.8\ m\ s^{-1}$ and different $a_{\_}$. (a) $a_{\_} = 2\ g$; (b) $a_{\_} = 2.5\ g$; (c) $a_{\_} = 3\ g$.

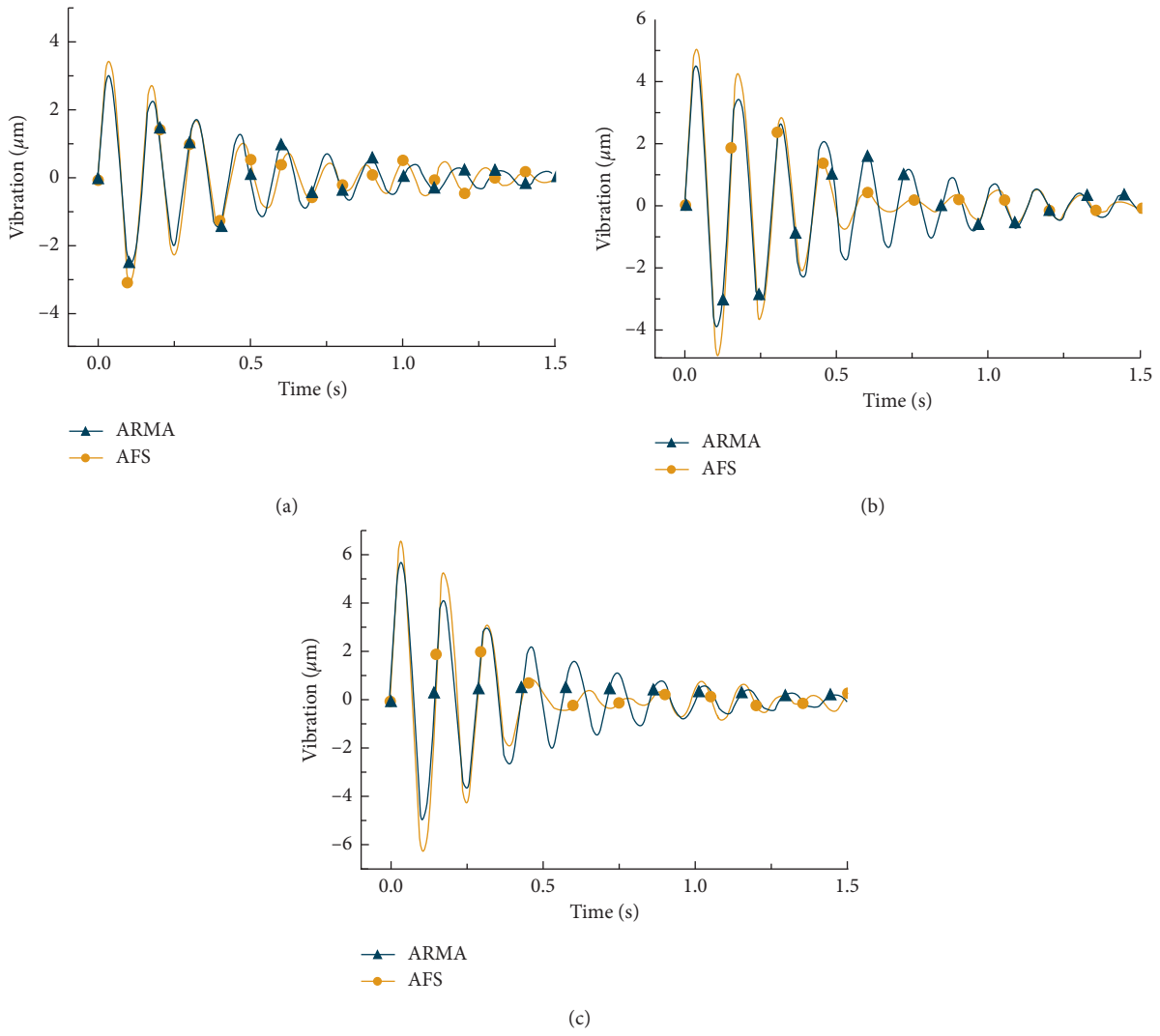

Figure 10: ARMA recognition results of trapezoidal move profile impact with $V_{max} = 0.3$ m s^{-1} and different a_. (a) $a_{\_} = 2$ g; (b) $a_{\_} = 2.5$ g; (c) $a_{\_} = 3$ g.

Table 2: ARMA recognition results of triangle move profile impact.

Acceleration $a_{\_}$ (g)	Undamped natural frequency w_n (rad/s)	Damping ratio ξ	Proportional coefficient λ
2	44.4233	0.04313	0.0048
2.5	44.5044	0.04063	0.0047
3	44.5379	0.04296	0.0049

Table 3: ARMA recognition results of trapezoidal move profile impact.

Acceleration $a_{\_}$ (g)	Undamped natural frequency w_n (rad/s)	Damping ratio ξ	Proportional coefficient λ
2	44.0291	0.04442	0.0048
2.5	44.8672	0.04219	0.0046
3	44.2201	0.05031	0.0049

It can be seen from the PSD diagram that the dominant mode frequency of the sample stage is about 7 Hz. In order to facilitate the identification of the system parameters, the band-pass filtering method is used to process the frequency band near the dominant mode. Then the frequency domain integration method is used to quadraticize the acceleration signal to obtain the displacement vibration signal of the residual vibration, which is used for the identification of system parameters. The ARMA method is used to identify the system model parameters. The results are presented in

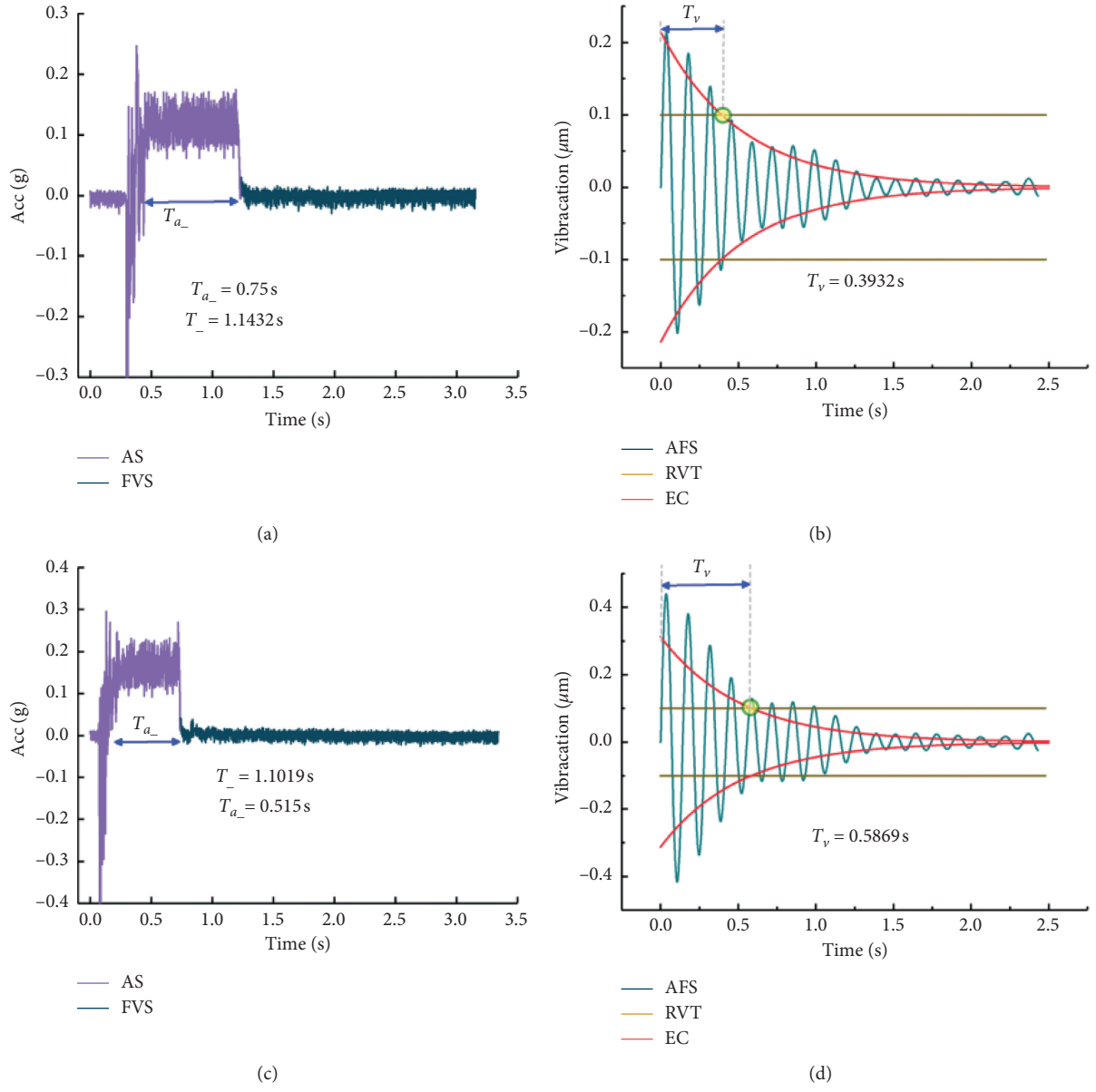

Figure 11: Continued.

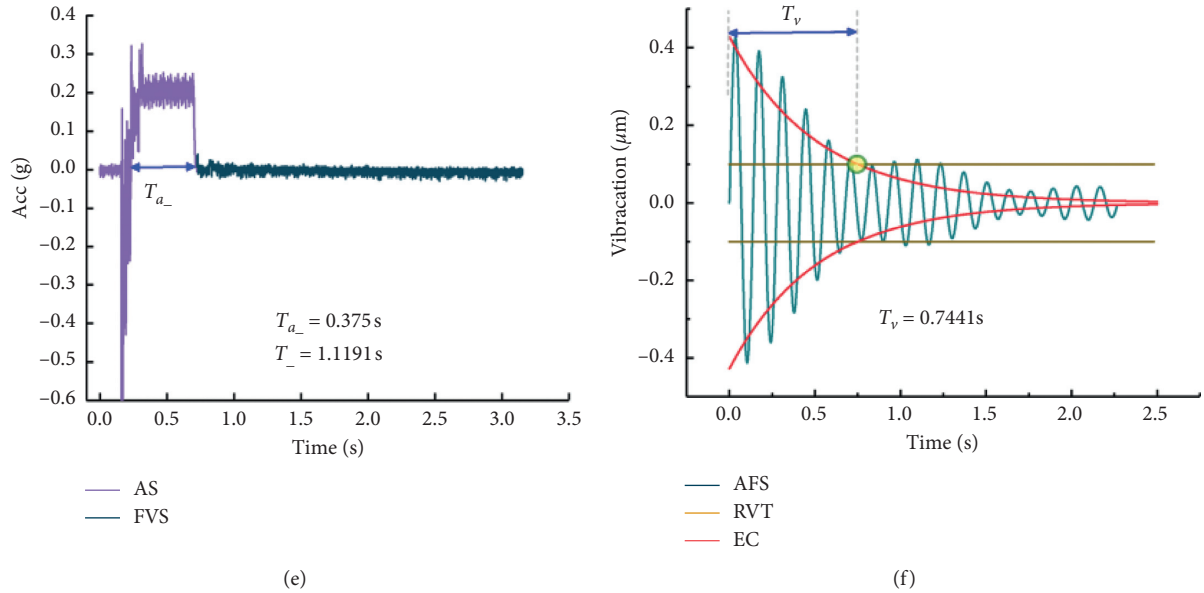

Figure 11: Residual vibration signal and corresponding delay time for different $a\_$ with $V_{\max} = 0.75\,\mathrm{m\,s^{-1}}$. (a) and (b) $a\_ = 1\,\mathrm{m\,s^{-2}}$, $T\_ = 1.1432$ s; (c) and (d) $a\_ = 1.46\,\mathrm{m\,s^{-2}}$, $T\_ = 1.1019$ s; (e) and (f) $a\_ = 2\,\mathrm{m\,s^{-2}}$, $T\_ = 1.1191$ s.

Figures 9 and 10. Figure 9 shows the ARMA residual vibration identification results under the triangular move profile and Figure 10 shows the ARMA residual vibration identification results under the trapezoidal move profile.

The natural frequency w_n and damping coefficient ξ of the sample stage identified in the two move profiles are shown in Tables 2 and 3. Finally, $w_n = 44.55$, $\xi = 0.04356$, and $\lambda = 0.004783$ are taken as the dynamic parameters of the sample stage.

It can be obtained from equation (31), when $w_n = 44.55$ and $\xi = 0.04356$, then $a\_ = 1.940598\ V_{\max}$. Assuming $V_{\max} = 0.75\,\mathrm{m\,s^{-1}}$, then the optimal acceleration of the deceleration section is $a\_ = 1.46\,\mathrm{m\,s^{-2}}$ and the deceleration section time is $T_{a\_} = 0.515$ s. The evaluated optimal delay time for laser irradiation is $T_v = 0.5850$ s, according to equation (28), which means the amplitude of the residual vibration will decay below the threshold when the decay time is greater than T_v. Figure 11 shows the experimental results when $a\_$ takes different values. The threshold of the residual vibration is set to 0.1 um. The results (Figures 11(c) and 11(d)) show that when $T_{a\_} = 0.515$ s, i.e., $a\_ = 1.46\,\mathrm{m\,s^{-2}}$, the experimental result of the T_v is 0.5869 s, which is very close to the evaluated optimal delay time. The time $T\_ = T_{a\_} + T_v = 1.1019$ s takes the minimum value, which proves the correctness of the conclusions in this paper. Obviously, this is useful for reducing the settling time and improving processing efficiency.

Although the difference in the values for $T\_$ between the three experiments is small, this is because the laser drilling machine of this paper uses a marble bed, which results in a smaller initial amplitude and a faster decay for the residual vibration. If the robotic arm or nonmarble bed structure of the laser processing equipment is used for positioning, the experimental results will be more obvious.

5. Conclusion

PTP motion is common in the industry. When the trapezoidal velocity trajectory is used in laser drilling, the sample stage will generate residual vibration when positioning completes. In order to reduce the influence of residual vibration on laser processing quality, it is necessary to set delay time to make the residual vibration attenuate, which causes a drop in overall machining efficiency. In this paper, based on the theoretical analysis, we have found that the acceleration value of the deceleration section for the trapezoidal moving profile can minimize the ST value, and the decay time after the sample stage positioning for laser irradiation can also be evaluated so that the whole laser drilling circle can be shorter.

The conclusions provided in this paper are simple and effective. Only the dynamic parameters of the sample stage are needed to obtain the optimal acceleration value of the deceleration section and the delay time for laser irradiation at a given operating speed, which effectively shortens the execution time of the whole laser drilling circle and improves the processing efficiency. In further research, the accurate acquisition methods of the dynamic parameters of the sample stage and the accurate time of the laser irradiation delay will be studied in more detail. At the same time, the conclusions of this paper will be applied to design the process instruction of large-area laser drilling and help to improve the overall drilling efficiency.

Data Availability

The data used to support the findings of this study are available from the corresponding author upon request.

Conflicts of Interest

Xiaodong Wang, Bin Liu, Xuesong Mei, Jun Yang, Xialun Yun, Xiao Li, and Jian Li declare that they have no conflicts of interest or financial conflicts to disclose.

Acknowledgments

This work was supported by the National Key Development Program of China (Grant nos. 2016YFB1102500 and 2016YFB1102602) and the National Natural Science Foundation of China (Grant no. 51735010).

References

[1] X. Wang, J. Cui, J. Zhang et al., "Simulation study of near-field enhancement on an Ag nanoparticle dimer system in a laser-induced nanowelding process," *Integrated Ferroelectrics*, vol. 191, no. 1, pp. 72–79, 2018.

[2] J. Cui, J. Zhang, X. He et al., "Atomistic simulations on the axial nanowelding configuration and contact behavior between Ag nanowire and single-walled carbon nanotubes," *Journal of Nanoparticle Research*, vol. 19, no. 3, p. 90, 2017.

[3] L. Yang, J. Cui, Y. Wang et al., "Nanospot welding of carbon nanotubes using near-field enhancement effect of AFM probe irradiated by optical fiber probe laser," *RSC Advances*, vol. 5, no. 70, pp. 56677–56685, 2015.

[4] A. Sharma and V. Yadava, "Experimental analysis of Nd-YAG laser cutting of sheet materials—a review," *Optics & Laser Technology*, vol. 98, pp. 264–280, 2018.

[5] Y. Liu, J. Deng, F. Wu, R. Duan, X. Zhang, and Y. Hou, "Wear resistance of carbide tools with textured flank-face in dry cutting of green alumina ceramics," *Wear*, vol. 372-373, pp. 91–103, 2017.

[6] S. Mishra, N. Sridhara, A. Mitra et al., "CO_2 laser cutting of ultra thin (75 μm) glass based rigid optical solar reflector (OSR) for spacecraft application," *Optics and Lasers in Engineering*, vol. 90, pp. 128–138, 2017.

[7] L. Yang, Y. Ding, M. Wang, T. Cao, and Y. Wang, "Numerical and experimental investigations on 342 nm femtosecond laser ablation of K24 superalloy," *Journal of Materials Processing Technology*, vol. 249, pp. 14–24, 2017.

[8] Z. Fan, X. Dong, K. Wang et al., "Effect of drilling allowance on TBC delamination, spatter and re-melted cracks characteristics in laser drilling of TBC coated superalloys," *International Journal of Machine Tools and Manufacture*, vol. 106, pp. 1–10, 2016.

[9] R. Wang, W. Duan, K. Wang et al., "Computational and experimental study on hole evolution and delamination in laser drilling of thermal barrier coated nickel superalloy," *Optics and Lasers in Engineering*, vol. 107, pp. 161–175, 2018.

[10] Z. Zhai, W. Wang, X. Mei et al., "Effect of temporal control of air/water environment on laser drilling of nickel-based alloy with thermal barrier coatings," *The International Journal of Advanced Manufacturing Technology*, vol. 97, no. 9–12, pp. 3395–3405, 2018.

[11] S. Marjanovic, G. A. Piech, S. Shanmugam et al., "Method for rapid laser drilling of holes in glass and products made therefrom," *US Patent, 9517963*, Corning Incorporated, Corning, NY, USA, 2016.

[12] R. Wang, K. Wang, D. Xia et al., "An experimental investigation into the defects of laser-drilled holes in thermal barrier coated inconel 718 superalloys," *The International Journal of Advanced Manufacturing Technology*, vol. 96, no. 1–4, pp. 1467–1481, 2018.

[13] B. Liu, G. Jiang, W. Wang et al., "Porous microstructures induced by picosecond laser scanning irradiation on stainless steel surface," *Optics and Lasers in Engineering*, vol. 78, pp. 55–63, 2016.

[14] B. Liu, W. Wang, G. Jiang et al., "Study on hierarchical structured PDMS for surface super-hydrophobicity using imprinting with ultrafast laser structured models," *Applied Surface Science*, vol. 364, pp. 528–538, 2016.

[15] A. Pan, W. Wang, B. Liu, X. Mei, H. Yang, and W. Zhao, "Formation of high-spatial-frequency periodic surface structures on indium-tin-oxide films using picosecond laser pulses," *Materials & Design*, vol. 121, pp. 126–135, 2017.

[16] K. Erkorkmaz, A. Alzaydi, A. Elfizy, and S. Engin, "Time-optimized hole sequence planning for 5-axis on-the-fly laser drilling," *CIRP Annals*, vol. 63, no. 1, pp. 377–380, 2014.

[17] N. Uchiyama, S. Sano, and K. Haneda, "Residual vibration suppression using simple motion trajectory for mechanical systems," *SICE Journal of Control, Measurement, and System Integration*, vol. 8, no. 3, pp. 195–200, 2015.

[18] H. Li, M. D. Le, Z. M. Gong et al., "Motion profile design to reduce residual vibration of high-speed positioning stages," *IEEE/ASME Transactions on Mechatronics*, vol. 14, no. 2, pp. 264–269, 2009.

[19] J. Chen, Q. Fang, and P. Li, "Effect of grinding wheel spindle vibration on surface roughness and subsurface damage in brittle material grinding," *International Journal of Machine Tools and Manufacture*, vol. 91, pp. 12–23, 2015.

[20] J. K. Myler, "The influence of machine tool vibration on the surface texture of diamond turned components," in *Proceedings of the 1st International Conference on Vibration Control in Optics and Metrology*, London, UK, February, 1987.

[21] Z. Hessainia, A. Belbah, M. A. Yallese, T. Mabrouki, J.-F. Rigal, and M. A. Yallese, "On the prediction of surface roughness in the hard turning based on cutting parameters and tool vibrations," *Measurement*, vol. 46, no. 5, pp. 1671–1681, 2013.

[22] K. Petrinec and Z. Kovacic, "Trajectory planning algorithm based on the continuity of jerk," in *Proceedings of the 2007 Mediterranean Conference on Control & Automation*, Athens, Greece, June 2007.

[23] J. Avalos and O. E. Ramos, "Optimal time-jerk trajectory generation for robot manipulators," in *Proceedings of the 2018 IEEE 2nd Colombian Conference on Robotics and Automation (CCRA)*, Barranquilla, Colombia, November 2018.

[24] J. Huang, P. Hu, K. Wu, and M. Zeng, "Optimal time-jerk trajectory planning for industrial robots," *Mechanism and Machine Theory*, vol. 121, pp. 530–544, 2018.

[25] P. Huang, Y. Xu, and B. Liang, "Global minimum-jerk trajectory planning of space manipulator," *International Journal of Control, Automation, and Systems*, vol. 4, no. 4, pp. 405–413, 2006.

[26] L. Ramli, Z. Mohamed, and H. I. Jaafar, "A neural network-based input shaping for swing suppression of an overhead crane under payload hoisting and mass variations," *Mechanical Systems and Signal Processing*, vol. 107, pp. 484–501, 2018.

[27] M. Ajayan and P. N. Nishad, "Vibration control of 3D gantry crane with precise positioning in two dimensions," in *Proceedings of the 2014 Annual International Conference on Emerging Research Areas: Magnetics, Machines and Drives (AICERA/iCMMD)*, Kottayam, India, July 2014.

[28] L. Biagiotti and R. Zanasi, "Open-loop and closed-loop filters for optimal trajectory planning under time and frequency

constraints," in *Proceedings of the Workshop on Robot Motion Planning: Online, Reactive, and in Real Time*, Vilamoura, Algarve, Portugal, October 2012.

[29] W. Singhose and J. Vaughan, "Reducing vibration by digital filtering and input shaping," *IEEE Transactions on Control Systems Technology*, vol. 19, no. 6, pp. 1410–1420, 2011.

[30] J. Bušek, M. Kuře, H. Martin, and T. Vyhlídal, "Control design with inverse feedback shaper for quadcopter with suspended load," in *Proceedings of the ASME 2018 Dynamic Systems and Control Conference*, Atlanta, Georgia, USA, September-October 2018.

[31] M. Hromcik and T. Vyhlidal, "Inverse feedback shapers for coupled multibody systems," *IEEE Transactions on Automatic Control*, vol. 62, no. 9, pp. 4804–4810, 2017.

[32] D. Pilbauer, T. Vyhlídal, and W. Michiels, "Spectral design of output feedback controllers for systems pre-compensated by input shapers," *IFAC-PapersOnLine*, vol. 48, no. 12, pp. 117–122, 2015.

[33] H. J. Yoon, S. Y. Chung, H. S. Kang, and M. J. Hwang, "Trapezoidal motion profile to suppress residual vibration of flexible object moved by robot," *Electronics*, vol. 8, no. 1, p. 30, 2019.

[34] X. Mao, H. He, H. Liu et al., "An approach of exciting CNC machine tools based on worktable empty running excitation," in *Proceedings of the 2017 3rd International Forum on Energy, Environment Science and Materials (IFEESM 2017)*, Shenzhen, China, November 2018.

[35] B. Li, B. Luo, X. Mao, H. Cai, F. Peng, and H. Liu, "A new approach to identifying the dynamic behavior of CNC machine tools with respect to different worktable feed speeds," *International Journal of Machine Tools and Manufacture*, vol. 72, pp. 73–84, 2013.

[36] D. K. Baek, T. J. Ko, and H. S. Kim, "Parameter identification for a single-degree-of-freedom system using autoregressive moving average model: application to cutting system," *Journal of Sound & Vibration*, vol. 295, no. 1-2, pp. 428–435, 2006.

[37] S. M. Pandit and S. M. Wu, *Time Series and System Analysis with Applications*, Wiley, New York, NY, USA, 1984.

[38] K. Erkorkmaz, A. Alzaydi, A. Elfizy, and S. Engin, "Time-optimal trajectory generation for 5-axis on-the-fly laser drilling," *CIRP Annals*, vol. 60, no. 1, pp. 411–414, 2011.